Bull. Chem. Soc. Ethiop. **2025**, 39(12), 2583-2592.
DOI: https://dx.doi.org/10.4314/bcse.v39i12.17

ISSN 1011-3924
Printed in Ethiopia
Online ISSN 1726-801X

IMPACT OF DEFECT-CONTAINING GRAPHENE OXIDE NANOSHEETS ON THE STRUCTURAL, ELECTRICAL, AND DIELECTRIC CHARACTERISTICS OF GRAPHENE OXIDE

Sundus Hadi Merza[1*]

[1]Department of Chemistry, College of Education for Pure Science / Ibn-Al-Haitham, University of Baghdad, Iraq

(Received December 30, 2024; Revised July 3, 2024; Accepted August 22, 2025)

ABSTRACT. In this work, two graphene oxide (GO) samples were prepared using the Hummers method with graphite (g) and $KMnO_4$ (g) ratios of 1:3 (GO_3) and 1:6 (GO_6). The effect of oxidation degree on the structural, electrical, and dielectric properties of the GO samples was investigated. The structures of the GO samples were studied using various techniques, including X-ray diffraction (XRD), Fourier transform infrared (FT-IR) spectroscopy, scanning electron microscopy (SEM), and energy-dispersive X-ray spectroscopy (EDXS). XRD analysis revealed an increase in the interlayer spacing and a decrease in the number of layers of the samples with increasing oxidant content. The two GO samples have giant permittivity values of ~10^5 in the low-frequency range. The characteristics of the functional groups and defects were clarified in terms of their high permittivity. The AC conductivity of the GO samples obeyed Jonscher's power law. The AC conductivities of GO_3 and GO_6 were calculated as 0.07 and 0.01 S/m at 1 MHz, respectively. The power exponent s has values in the range $0 < s < 1$. In addition, a low loss tangent was observed for GO_6 in the high-frequency range.

KEY WORDS: Jonscher's power law, AC conductivity, Defect, Permittivity, Loss tangent, Graphene oxide

INTRODUCTION

Graphene oxide (GO) is a two-dimensional (2D) material composed of C atoms bonded in hexagons. It is prepared via the strong oxidation of graphite [1]. GO contains various oxygenated functional groups, such as OH, COOH, C=O, and epoxy groups, on its edge and basal planes. These oxygen functional groups (OFG) allow GO to disperse in polar solvents and aqueous solutions [2]. FG serves as a starting site for various functionalities, enabling a wide range of applications [3]. Indeed, as graphite is exfoliated by the Hummer, Staudenmaier, or Brodie method, structural defects are introduced. For instance, the sp^2 hybridization of graphene flakes changes to sp^3, lengthens the C-C bond, and forms holes, vacancies, grain boundaries, and edge dislocations [4]. These defects can enhance the material's polarizability, thereby improving its dielectric properties. Dielectric properties describe how a material interacts with an electric field, particularly its ability to store or dissipate electrical energy. The relative permittivity and dielectric loss are the core components of the material's dielectric properties. Carbonaceous materials such as GO, RGO, and exfoliated graphite have been explored and found to exhibit exceptionally high permittivity values [5-7]. This study offers new insights into the impact of oxidation level on the dielectric behavior of GO, employing graphite to $KMnO_4$ ratios of 1:3 and 1:6. The findings emphasize the potential of high-dielectric-constant materials for advanced applications in energy storage, modern microelectronics, sensors, and multifunctional devices [8]. The prepared GO samples were characterized by Fourier transform infrared (FT-IR) spectroscopy, scanning electron microscopy (SEM), energy-dispersive X-ray spectroscopy (EDXS), and X-ray diffraction (XRD).

*Corresponding author. E-mail: sundus.h.m@ihcoedu.uobaghdad.edu.iq

EXPERIMENTAL

Materials and apparatuses

Graphite flake (GT) was used to synthesize GO from Fluka. In addition, H_2SO_4 98% and HNO_3 were purchased from THOMAS BAKER and GCC company, respectively. Also, $KMnO_4$, H_2O_2, and $NaNO_3$ were obtained from BHD, Dagenham, and Fluka, respectively. Cu-K_α radiation was employed in the X-Ray Diffractometer (XRD-6000, SHIMADZU-Japan) to investigate the interlayer spacing and structural properties of the samples. The morphology and elemental composition were provided by SEM (MIRA3 TESCAN, Czech) and EDX spectroscopy (X-max, Oxford, England). To obtain chemical structural information, a Shimadzu FT-IR spectrophotometer was used. The infrared spectra were recorded in the region 400-4000 cm^{-1} using KBr pellets.

Synthesis of GO

The Hummer method was used to synthesize the GO [9]. According to this method, 23 mL of 98% H_2SO_4 was combined with 1 g of graphite (GT) and 0.5 g of $NaNO_3$ in an ice bath for 30 min. Thereafter, 3 g of $KMnO_4$ was gradually and cautiously added to prevent the temperature from rising above 20 °C. After removing the ice bath, the temperature was raised to 35 ± 3 °C and held there for 30 min. In the second step, 46 mL of H_2O was added to raise the temperature to 98 °C within 15 min. The suspension was brown. The suspension was diluted with 140 mL of warm water and then treated with 30% H_2O_2 to eliminate colorless and soluble manganese sulfate. The warm suspension was then treated with a 5% HCl solution, followed by rinsing with distilled water until the pH reached 7. The dried filter cake was obtained after 48 hours of drying in a vacuum oven. GO samples were obtained using two weight ratios of graphite to potassium permanganate: 1:3 (GO_3) and 1:6 (GO_6).

Fabrication of GO pellets for the dielectric measurements

GO_3 and GO_6 were pressed into pellets using a 400-bar hydraulic press. To measure their dielectric behavior, the pellet was kept dry to prevent moisture absorption. The dielectric measurements were conducted using an LCR meter within the electromagnetic frequency range of 50 Hz to 1 MHz. The relative permittivity (ε'), imaginary permittivity (ε''), loss tangent, and AC conductivity of the two samples were calculated from the resistance (R) and capacitance (C) measurements. The dimensions of the resultant pellets, GO_3 and GO_6, were 10 mm in diameter, and their thicknesses were measured using a vernier caliper to be 2.45 and 2.69 mm, respectively.

RESULT AND DISCUSSION

Characterization of the synthesized materials

X-ray diffraction (XRD): XRD pattern of graphite (GT) flake (Figure 1a) displays distinct diffraction peaks at 26.57º, 44.36º, and 54.59º, corresponding to the planes (002), (101), and (004), respectively. The XRD pattern for GT was compared with the literature data (CAS Number 7782-42-5) [10]. Two graphitic peaks of GO_3 and GO_6 (Figure 1b) were observed at $2\theta = 10.08^\circ$ and 8.09° with interlayer spacing (d) = 0.8763 nm and 1.098 nm, respectively. The increase in interlayer spacing of GO_6 and the formation of a graphitic peak with lower intensity than that of GO_3 indicate the intercalation of many oxygen functional groups (OFGs) within the graphite lattice.

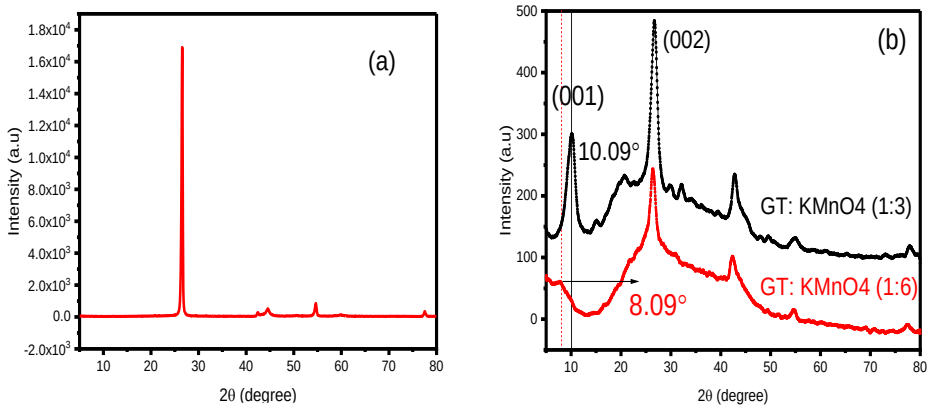

Figure 1. XRD pattern of (a) GT (b) GO_3 and GO_6.

The thickness (t) of GO_3 and GO_6 was calculated using the classical Debye-Scherrer equation [11,12].

$$t = \frac{0.94\,\lambda}{\beta_D \cos\theta} \quad (1)$$

Where β_D is the full width at half maximum (FWHM) in radians, θ is the diffraction angle, 0.94 is a shape factor, and λ is the wavelength of X-rays used (1.543 Å). The average number of layers (n) in GT, GO_3, and GO_6 was calculated by dividing the thickness by the interlayer spacing (d). The XRD data for the GT and GO samples were compared with those from other studies (Table 1). According to Table 1, GO_6 has fewer layers and a higher d-spacing than GO_3 and other studies, suggesting that the oxidation conditions led to enhanced exfoliation and greater disruption of the graphene oxide stack. These structural features can significantly affect their properties and potential energy storage applications. From the outcome, it could be concluded that the procedure proposed was effective in exfoliating the layers of the GO samples.

Table 1 XRD data for GT, GO_3, and GO_6 compared with other studies.

Samples	(2θ) degree	Interlayer spacing (d) (nm)	FWHM (degree)	Thickness (nm)	n	Method
This work	GT (26.57°)	0.33	0.31	33.7262	100.6	-
	GO_3 (10.08°)	0.87	1.73	4.5651	5.20	Hummer
	GO_6 (8.09°)	1.09	1.56	5.0556	4.6	
[13]	11°-12°	0.74 - 0.81	-	11-13	-	Hummer
[1]	11.95°	0.73	-	-	-	Hummer
[14]	10.9°	0.81	-	-	-	Improved hummer
[15]	9.2°	0.96	-	-	4	Sonication
[16]	9.91°	0.89	-	-	4-5	Tour

FESEM and EDXS analysis.

The surface morphology and elemental composition of GT, as well as those of synthesized GO_3 and GO_6, were examined using FESEM and EDXS. FESEM analysis (Figure 2a) revealed that GT exhibits a prominent morphology categorized by thick and moderately large flakes, exhibiting

a discrete planar structure. The individual flakes appear less wrinkled and exhibit smoother basal planes than typical GO samples. In contrast, both GO_3 and GO_6 (Figure 2b, c) exhibit exfoliated, wrinkled layer morphologies due to oxidation. EDXS analysis confirmed that all samples (GT, GO_3, and GO_6 are primarily composed of C and O atoms. Notably, an increase in $KMnO_4$ dosage led to a greater number of oxygen-containing groups and, consequently, a higher oxygen percentage in GO_6 relative to GT and GO_3.

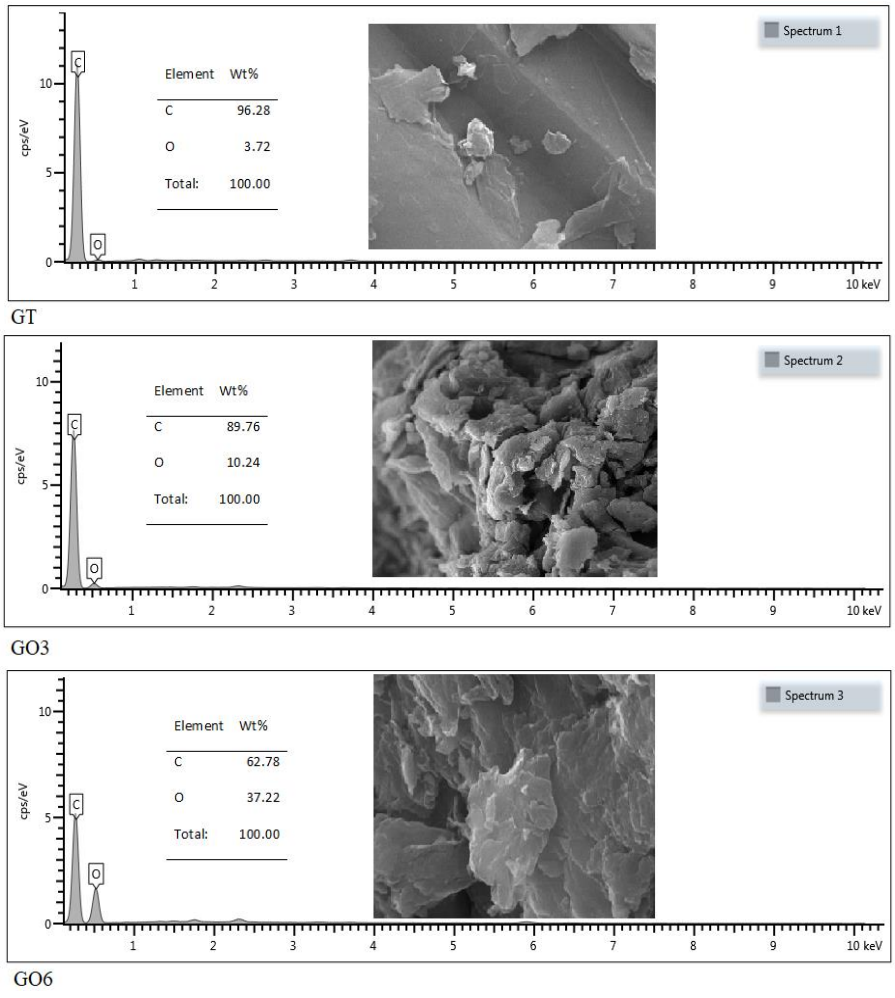

Figure 2. EDXS *spectra and SEM images for* GT(a), GO_3 (b) and GO_6 (c).

FT-IR spectra for the synthesized materials

Figure 3 presents the FT-IR spectra for GT, GO_3, and GO_6. The FTIR spectrum of GT shows only a few peaks of very low intensity, possibly due to adsorbed moisture or minor functionalization. In contrast, GO_6 shows a firm characteristic peak at 1061 cm^{-1}, which corresponds to the stretching vibration of epoxy and/or secondary alcohol groups. Additionally, a peak at 1736 cm^{-1} is attributed to carbonyl groups, and another at 1379 is assigned to the C–O bond within carboxyl groups

[5,17,18]. The absorption peaks at 2908 cm^{-1} and 2849 cm^{-1} are characteristic of asymmetric and symmetric stretching vibration of aliphatic C-H, respectively. These peaks indicate an increase in oxygen-containing functional groups and a higher proportion of carbon atoms adopting sp^3 hybridization within the GO_6 structure. Furthermore, a broad and strong absorption band observed in the 3100-3700 cm^{-1} region is attributed to the OH stretching vibration [18]. The notable peak observed in GO_6 at 1617 cm^{-1} is likely due to bending vibrations of OH groups within its layers and to H_2O molecules trapped within oxidized layers. This observation reflects the enhanced hydrophilic nature of the GO layers [19]. The peak at 1550 cm^{-1} is likely attributed to the stretching vibration of aromatic C=C bonds [19]. The increased intensity of all these peaks in GO_6 compared to GO_3 and GT indicates a higher concentration of oxygen-containing functional groups in its structure, suggesting a more effective oxidation process at the 1:6 oxidant ratio than at 1:3.

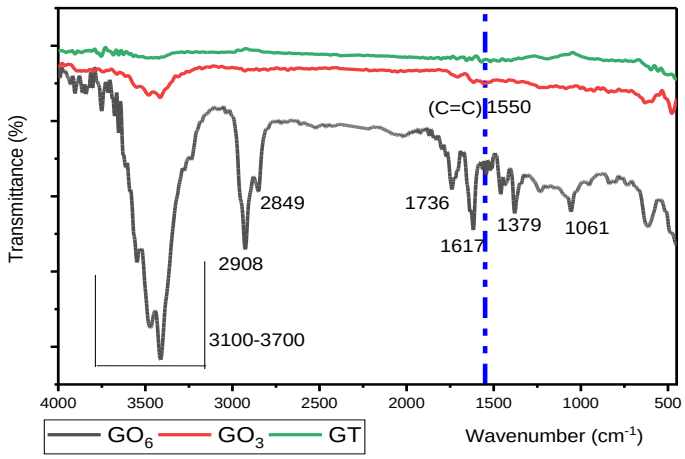

Figure 3. FT-IR for the synthesized GO_3, GO_6 and GT.

LCR measurement for the synthesized materials

The permittivities of GO_3 and GO_6 were calculated at ambient temperature over the frequency range of 50 Hz – 1 MHz. The permittivity is the ratio of the capacitance (C) of a substance in Farad to the capacitance of space or without medium C_o. The relative permittivity is calculated using the following equation:

$$\varepsilon = \frac{C}{C_0} \tag{2}$$

Where C_0 is equal to the following formula:

$$C_0 = \frac{\varepsilon_\circ A}{d} \tag{3}$$

Subsequently, the ε can be determined utilizing the following equation: [20, 3]

$$\varepsilon = \frac{C\,d}{\varepsilon_\circ\,A} \tag{4}$$

Where (d), (ε), and (A) stand for pellet thickness in meters, permittivity of free space 8.854× 10^{-12} $F.m^{-1}$, and pellet area (m^2), respectively. Figure 4 shows the frequency dependence of ε for GO_3 and GO_6. At low frequency, ε is observed to be 1.46×10^5 for GO_3 and 1.26×10^5 for GO_6. Both GO_3 and GO_6 have giant permittivity. The ε for graphite is 53.3± 1.3 [7]. The theory put forward by Koop, in combination with Maxwell-Wagner's model of interfacial polarization,

can help explain this behavior. The charge accumulation from the functional groups of GO_3 and GO_6 created a separation between the conductive grains and the non-conductive grain boundaries, represented by defects (functional groups and vacancies), thereby enhancing polarization and increasing ε. It is also important to note that, because electric dipoles are unable to keep up with the rapid fluctuations in the applied field, ε falls sharply with increasing frequency and then becomes almost frequency-independent [3].

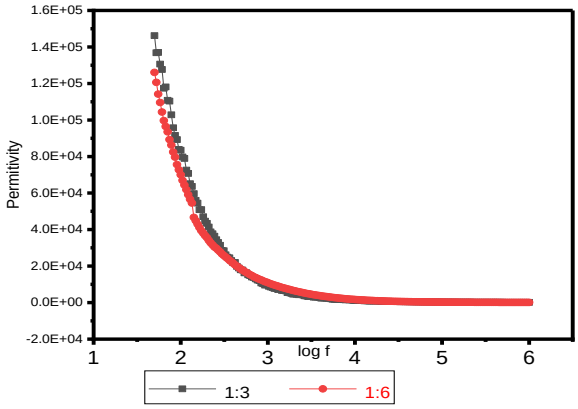

Figure 4. The relative permittivity of GO_3 and GO_6 versus frequency.

The imaginary permittivity (ε") is employed to assess the dielectric loss and was calculated using the following formula:

$$\varepsilon'' = \frac{d}{R\,A\,\omega\varepsilon_\circ} \tag{5}$$

Where R and A represent the resistance and electrode area (m^2), respectively, and ω represents the angular frequency, defined as $\omega = 2\pi f$. Both GO_3 and GO_6 (Figure 5a) exhibit high values of the ε″ at lower frequencies, then decrease as the frequency rises. At low frequencies, the low conductivity at grain boundaries requires more energy for charge-carrier movement, leading to higher dielectric loss. In contrast, at high frequencies, the higher conductivity of grain boundaries requires less energy for charge-carrier movement, leading to lower dielectric loss values. Furthermore, the ε" is made up of two factors: conductivity loss (σ/ω) and dielectric loss (ε"). Since the conductivity loss values for GO_3 and GO_6 were less than 1, it has been established that these materials are dielectric.

The loss tangent (tan δ), Equation 6, is a crucial number in mechanical and electrical applications. It is proportional to the power dissipated as heat to the material's stored energy [20].

$$tan\,\delta = \frac{\varepsilon''}{\varepsilon'} \tag{6}$$

Where the angle δ represents the phase difference that has developed between the applied and induced electric fields. Figure 5b illustrates how the tan δ varies with the frequency for GO_3 and GO_6 in the 50 Hz–1 MHz range. The tan δ value decreases consistently with increasing frequency, and GO_6 exhibits lower values compared to GO_3 at various frequencies: at 50 Hz (4.35 vs. 168.23), 1 kHz (4.07 vs. 136.56), 10 kHz (3.75 vs. 104.36), 100 kHz (3.41 vs. 44.38), and 1 MHz (2.31 vs. 9.79). The tan δ responses of GO_3 and GO_6 showed a relaxation peak, indicating the presence of a relaxing dipole. Low tan δ values are desirable for the dielectric material in a dielectric capacitor.

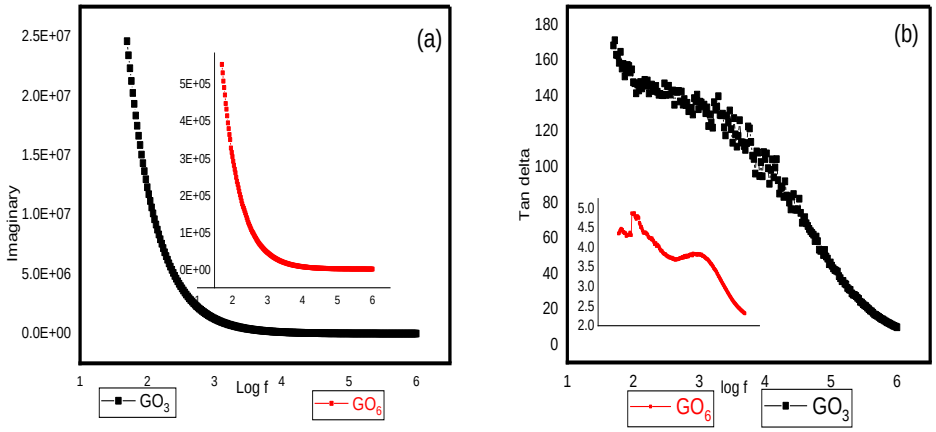

Figure 5. Imaginary permittivity (a) and loss tangent (b) of GO_3 and GO_6 as a function of frequency at ambient temperature.

From the LCR meter, the total conductivity $\sigma_{t(\omega)}$ was calculated from the measured resistance R using Equation 7.

$$\sigma_{t(\omega)} = \frac{d}{R\,A} \tag{7}$$

The total conductivity $\sigma_{t(\omega)}$ was calculated using the equation below.

$$\sigma_{t(\omega)} = \sigma_{ac(\omega)} + \sigma_{dc(0)} \tag{8}$$

where σ_{dc} is the DC conductivity that can be determined from extrapolated σ_{ac} to the lowest measured frequency (f→0). σ_{dc} is independent of frequency and depends on the mobility of free charge carriers. $\sigma_{ac(\omega)}$ is the AC conductivity and depends on frequency. The $\sigma_{ac(\omega)}$ can be referred to as the universal dynamic form of AC conductivity proposed by Jonscher, where $\sigma_{ac(\omega)} = A\omega^s$. Where A is the strength of polarizability and is dependent on temperature and composition, ω is the angular frequency, and s is the frequency exponent that can take the value range of $0 < s < 1$, which describes the degree of interaction between charge carriers and the surrounding lattices [21, 22]. The non-linear fitting of Jonscher's equation is illustrated in Figure 6. As shown in Figure 6, the AC conductivity increases with frequency for both GO_3 and GO_6, indicating that the materials exhibit frequency-dependent behavior. Additionally, as frequency increases, free charge carriers may hop between localized electronic states due to the presence of oxygen-containing groups and structural defects, thereby increasing overall electrical conduction [23]. The parameters A, exponent s and σ_{dc} values of GO_3 are 1.71754×10^{-4}, 0.22016 and $0.06819 \pm 8.8574\times 10^{-5}$while for GO_6 are 6.49421×10^{-5}, 0.30682 ± 0.00675 and $0.00142 \pm 5.4425\times10^{-5}$, respectively.

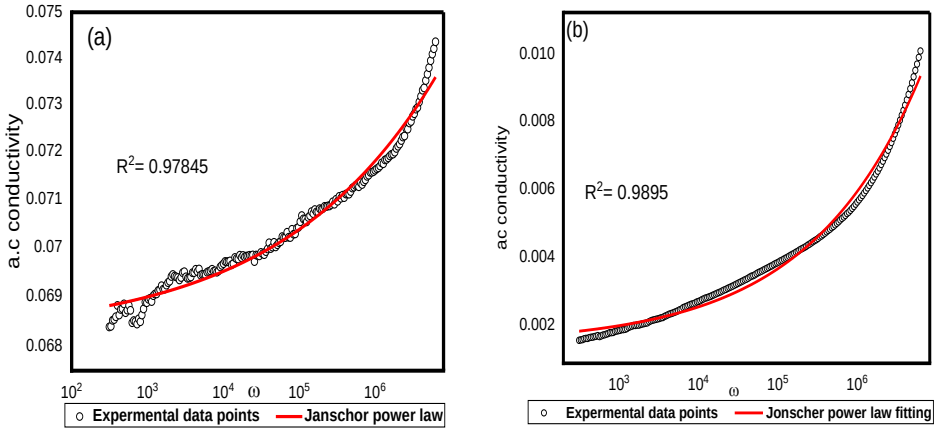

Figure 6. Nonlinear Jonscher's law fitting for (a) GO_3 and (b) GO_6.

In the high-frequency region, since A $\omega^s \gg \sigma_{dc(0)}$, so the $\sigma_{t(\omega)}$ is equal to the $\sigma_{ac(\omega)}$ [24]. The dependence of the $\sigma_{ac(\omega)}$ of GO_3 and GO_6 on the frequency can be studied based on the linear Jonscher's power law, $ln\ \sigma_{ac} = ln\ A + s\ ln\ \omega$. The values of A and the exponent s for GO samples were obtained from the intercept and slope, respectively, of the linear plot of $\ln(\sigma_{ac})$ vs. $\ln(\omega)$ (Figure 7). The parameters A and s from the linear Jonscher's power law were determined to be 0.0657 and 0.0064 for GO_3 and 0.00053 and 0.1733 for GO_6, respectively. The estimated exponent s was found to be less than unity for both samples, indicating that the AC conductivity is frequency-dependent and supporting the presence of a charge-carrier hopping mechanism [25].

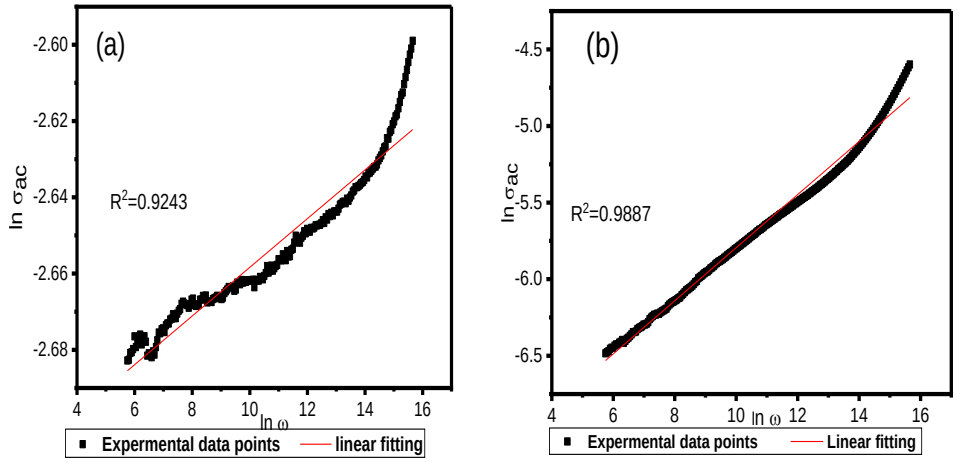

Figure 7. Plot of $\ln(\sigma_{ac})$ vs. $\ln(\omega)$ for (a) GO_3 and (b) GO_6.

CONCLUSION

In this work, two samples of few-layered graphene oxide (GO) were successfully synthesized using the Hummers method. The FT-IR analysis revealed the presence of various oxygen functional groups, including carboxyl, epoxy, and hydroxyl, confirming the successful oxidation of graphite. XRD analysis showed an increase in the interlayer spacing of the GO_3 and GO_6 samples compared to graphite (GT), indicating effective oxidation and exfoliation. SEM micrographs further revealed that the flakes were unstacked, demonstrating the effective disruption of the graphite structure. Both GO_3 and GO_6 exhibited high relative permittivity values, on the order of 10^5, which can be attributed to the high defect density and oxygen functional groups present in the materials. Notably, GO_6 exhibited a lower loss tangent at high frequencies, suggesting improved dielectric performance in specific applications. Additionally, the AC conductivity of both GO_3 and GO_6 increased with frequency and followed Jonscher's power law. These structural and electrical properties of the synthesized graphene oxide samples demonstrate their suitability for various advanced applications, particularly in electronics and energy storage, where high dielectric performance and tunable conductivity are critical.

ACKNOWLEDGMENT

The authors are grateful for the support from the Department of Chemistry, College of Pure Science (Ibn Al-Haitham), University of Baghdad.

REFERENCES

1. Latif, I.A.; Merza, S.H. Effect of scan rate and pH on determination amoxilline using screen printed carbon electrode modified with functionalized graphene oxide. *Ibn AL-Haitham J. Pure Appl. Sci.* **2018**, 31, 157-171.
2. Johnson, D.W.; Dobson, B.P.; Coleman, K.S. A manufacturing perspective on graphene dispersions. *Curr. Opin. Colloid Interface Sci.* **2015**, 20, 367-382.
3. Neelam, S.; Thida, R.; Chidurala, S.C.; Daripaalli, S.; Butreddy, R.R. Enhanced structural and electrochemical properties of spinel structured Ca doped nickel cobaltite nanoparticles synthesized by microwave hydrothermal method. *Int. J. Eng. Res. Appl.* **2023**, 13, 29-41.
4. Sun, Y.; Tang, X.; Bao, H.; Yang, Z.; Ma, F. The effects of hydroxide and epoxide functional groups on the mechanical properties of graphene oxide and its failure mechanism by molecular dynamics simulations. *RSC Adv.* **2020**, 10, 29610-29617.
5. Kumar, K.S.; Pittala, S.; Sanyadanam, S.; Paik, P. A new single/few-layered graphene oxide with a high dielectric constant of 106: Contribution of defects and functional groups. *RSC Adv.* **2015**, 5, 14768-14779.
6. Hong, X.; Yu, W.; Chung, D.D.L. Electric permittivity of reduced graphite oxide. *Carbon* **2017**, 111, 182-190.
7. Hong, X.; Chung, D.D.L. Exfoliated graphite with relative dielectric constant reaching 360, obtained by exfoliation of acid-intercalated graphite flakes without subsequent removal of the residual acidity. *Carbon* **2015**, 91, 1-10.
8. Gonçalves, M.G.; Costa, V.O.; Martinez, A.H.G.; Régnier, B.M.; Gomes, G.C.B.; Zarbin, A.J.G.; Orth, E.S. Functionalization of graphene oxide via epoxide groups: A comprehensive review of synthetic routes and challenges. *Frontiers in Carbon* **2024**, 3, 1-22.
9. Merza, S.H. and I. latif. *Synthesis of Modified Graphene Oxide and Its Application as Electrochemical Sensor*. PhD thesis, University of Baghdad, Baghdad, Iraq, **2017**.
10. Güzel, T. Investigation of the usability of nitric acid electrolyte in graphene production by electrochemical method. *Fuller. Nanotub. Carbon Nanostructures* **2020**, 29, 175-182.

11. Abduljabar, M.A.; Merza, S. Graphene oxide decorated with nickel cobaltite nanoparticles as an adsorbent for cationic methyl green dye: Kinetic, isotherm, and thermodynamic studies. *Baghdad Sci. J.* **2024**, 21, 2853-2865.
12. Nagham H.A.; Sundus H.M. Preparation, kinetics, and thermodynamic investigation of Janus green dye removal from aqueous solutions using MnO_2 nanoparticles as an adsorbent. *Bull. Chem. Soc. Ethiop.* **2025**, 39, 1509-1523
13. Karnis, I.; Krasanakis, F.; Sygellou, L.; Rissanou, A.N.; Karatasos, K.; Chrissopoulou, K. Varying the degree of oxidation of graphite: Effect of oxidation time and oxidant mass. *Phys. Chem. Chem. Phys.* **2024**, *26*, 10054-10068.
14. Chen, J.; Yao, B.; Li, C.; Shi, G. An Improved hummers method for eco-friendly synthesis of graphene oxide. *Carbon* **2013**, 64, 225-229.
15. Bera, M.; Chandravati; Gupta, P.; Maji, P.K. Facile one-pot synthesis of graphene oxide by sonication assisted mechanochemical approach and its surface chemistry. *J. Nanosci. Nanotechnol.* **2017**, 18, 902-912.
16. Fatmawati, D.A.; Triyono, T.; Trisunaryanti, W.; Oktaviano, H.S.; Chasanah, U. The influence of permanganate enhancement to graphite on chemical structure and properties of graphene oxide material generated by improved tour method. *Indones. J. Chem.* **2021**, 21, 1086-1096.
17. Emiru, T.F.; Ayele, D.W. Controlled synthesis, characterization and reduction of graphene oxide: A convenient method for large scale production. *Egypt. J. Basic Appl. Sci.* **2017**, 4, 74-79.
18. Foster, M.; Eutilério, Ch.; Imasiku, N.; Eric, M.; Heidi, R.; Luke, Ch. Risk assessment of selected endocrine disrupting compounds in selected raw foodstuffs sold on open markets in Zambia. *Bull.Chem. Soc. Ethiop.* **2025**, 39, 1227-1244.
19. Oliveira, L.S.; Alba, J.F.G.; Silva, V.L.; Ribeiro, R.T.; Falcão, E.H.L.; Navarro, M. The effect of surface functional groups on the performance of graphite powders used as electrodes. *J. Electroanal. Chem.* **2018**, 818, 106-113.
20. Merza, S.H.; Mousa, E.F. Dielectric properties of ultra-low dielectric constant PVA-pentaerythritol/MnO_2 nanocomposite. *Phys. Chem. Res.* **2022**, 10, 325-331.
21. Abdel–Baset, T.A.; Belhaj, M. Structural characterization, dielectric properties and electrical conductivity of ZnO nanoparticles synthesized by co-precipitation route. *Physica B: Condensed Matter* **2021**, 616, 1-6.
22. Ahamad, T.; Ahmed, A.S. Influence of graphene oxide on the dielectric properties of biogenically synthesized ZnO nanoparticles. *Hybrid Adv.* **2023**, 3, 1-15.
23. Sagadevan, S.; Pal, K.; Chowdhury, Z.Z.; Hoque, M.E. Structural, optical and dielectric investigation of $CdFe_2O_4$ nanoparticles. *Mater. Res. Express* **2017**, 4, 1-13.
24. Stavrakas, I.; Moutzouris, K.; Ninos, K.; Mitritsakis, N.; Agioutantis, Z.; Triantis, D. Using AC conductivity measurements to study the influence of mechanical stress on the strength of geomaterials. *Open J. Appl. Sci.* **2012**, 02, 61-65.
25. Abushad, M.; Arshad, M.; Naseem, S.; Husain, S.; Khan, W. Role of Cr doping in tuning the optical and dielectric properties of TiO_2 nanostructures. *Mater. Chem. Phys.* **2020**, 256, 1-12.